




Article

Radiomic-Based Biomarkers for the Evaluation of Prosthetic Heart Valve Infective Endocarditis in Non-Attenuation Correction [¹⁸F]FDG PET/CT Images

David Palomino-Fernández ¹, Adolfo Gómez-Grande ^{2,3}, Alexander P. Seiffert ¹, Héctor Bueno ^{3,4,5,6}, Enrique J. Gómez ^{1,7} and Patricia Sánchez-González ^{1,7,*}

- ¹ Biomedical Engineering and Telemedicine Centre, ETSI Telecomunicación, Center for Biomedical Technology, Universidad Politécnica de Madrid, 28040 Madrid, Spain; david.palomino.fernandez@alumnos.upm.es (D.P.-F.); ap.seiffert@upm.es (A.P.S.); enriquejavier.gomez@upm.es (E.J.G.)
 - ² Department of Nuclear Medicine, Hospital Universitario 12 de Octubre, 28041 Madrid, Spain; adolfo.gomez@salud.madrid.org
 - ³ Centro Nacional de Investigaciones Cardiovasculares (CNIC), 29029 Madrid, Spain; hector.bueno@cnic.es
 - ⁴ Cardiology Department, Instituto de Investigación Sanitaria (imas12), Hospital Universitario 12 de Octubre, 28041 Madrid, Spain
 - ⁵ Centro de Investigación Biomédica en Red de Enfermedades Cardiovasculares (CIBERCV), 28029 Madrid, Spain
 - ⁶ Facultad de Medicina, Universidad Complutense de Madrid, 28040 Madrid, Spain
 - ⁷ Centro de Investigación Biomédica en Red de Bioingeniería, Biomateriales y Nanomedicina, Instituto de Salud Carlos III, 28029 Madrid, Spain
- * Correspondence: p.sanchez@upm.es; Tel.: +34-910-672-477

Abstract: Although there have been crucial advancements in the diagnostic and treatment approaches, the mortality rate of infective endocarditis is still an ongoing challenge in clinical practice. [¹⁸F]FDG PET/CT imaging has recently proven its potential role in the early identification of prosthetic valve endocarditis (PVE). Due to radiomics' rising applicability, recent studies exhibit promising outcomes in the clinical setting. The aim of the present study is the evaluation of potential radiomic-based biomarkers of non-attenuation-corrected (NAC) [¹⁸F]FDG PET images for the diagnosis of PVE. An adequate pre-processing and segmentation of the prosthetic ring metabolic activity were performed. A reproducibility analysis prior to the image-based biomarkers' identification was conducted in terms of the intraclass correlation coefficient (ICC) derived from the variations in the radiomic extraction configurations (bin number and voxel size). After the reliability analysis, statistical analysis was performed by means of the Mann–Whitney U Test to study the differences between the PVE groups. Only *p* values < 0.05 after the Benjamini Hochberg correction procedure for multiple comparisons were considered statistically significant. Eight ML classification models for PVE classification based on radiomic features were evaluated. Overall, 45.2% and 95.7% of the radiomic features showed a consistency ICC above 0.82, demonstrating great reproducibility against variations in the bin number and interpolation thickness, respectively. Variations in interpolation thickness demonstrated great reproducibility in absolute agreement with 80.0% robust features, proving a non-dependency relationship with radiomic values. In the present study, the utility of potential radiomic-based biomarkers in the diagnosis of PVE in NAC [¹⁸F]FDG PET/CT images has been evaluated. Future studies will be required to validate the use of this technology as a valuable tool to support the current PVE diagnostic criteria.

Keywords: infective endocarditis; [¹⁸F]FDG PET/CT; reproducibility analysis; radiomics; machine learning



Citation: Palomino-Fernández, D.; Gómez-Grande, A.; P. Seiffert, A.; Bueno, H.; J. Gómez, E.; Sánchez-González, P. Radiomic-Based Biomarkers for the Evaluation of Prosthetic Heart Valve Infective Endocarditis in Non-Attenuation Correction [¹⁸F]FDG PET/CT Images. *Appl. Sci.* **2024**, *14*, 2296. <https://doi.org/10.3390/app14062296>

Academic Editor: Grazia Maria Virzi

Received: 8 February 2024

Revised: 5 March 2024

Accepted: 7 March 2024

Published: 8 March 2024



Copyright: © 2024 by the authors. Licensee MDPI, Basel, Switzerland. This article is an open access article distributed under the terms and conditions of the Creative Commons Attribution (CC BY) license (<https://creativecommons.org/licenses/by/4.0/>).

1. Introduction

Infective endocarditis (IE) is a pathological condition in the heart derived from the proliferation of microorganisms causing inflammatory disease involving the heart valves [1]. It is a diagnostic challenge due to the high variability of the presentation of clinical signs. The current diagnosis is a compendium of microbiological information and medical imaging, interpreted in combination with clinical signs and symptoms. This information is included as part of the criteria that define the gold standard of diagnosis, the modified Duke criteria. These criteria classify endocarditis into three subcategories based on the aforementioned findings: rejected, possible, and definite IE [2,3]. However, these criteria exhibit limited sensitivity and specificity [4–6], as reported in the most recent AHA/IDSA and ESC guidelines [3,7]. Despite the vast comprehension of IE clinical management, the morbimortality of this disease is still unacceptably high (20% at 30 days and 40–50% at subsequent follow-up) due to consequent complications [8].

The early identification of signs is crucial in preventing future complications and thus reducing the associated morbidity and mortality. The transthoracic (TTE) and transesophageal ultrasound (TEE) are usually employed as the gold standard in the diagnosis of IE. However, TTE especially fails to identify approximately 30% of the cases with prosthetic valve endocarditis (PVE) or infections in implantable electronic devices (CIED) [8]. In fact, when echocardiography fails to detect infective valve endocarditis, the Duke criteria show reduced diagnostic sensitivity [8]. Moreover, the sensitivity of echocardiography is still limited depending on several factors related to the stage of the disease, the clinician's expertise, or even the prosthetic material-related imaging artifacts. This limited sensitivity of diagnostic procedures leads to an important delay in the early diagnosis and consequent structural damage due to the infection [4,9]. Precisely because of the limitations found in the modified Duke criteria, especially in the context of PVE and cardiovascular device-related infective endocarditis (CDRIE), additional imaging modalities were introduced as part of the ESC guideline criteria. In particular, the AHA guidelines recently highlighted the potential of the ^{18}F FDG PET/CT imaging in the diagnosis of PVE and native valve endocarditis (NVE) [7]. ^{18}F FDG PET/CT imaging has demonstrated a major role in PVE for the identification of valvular and perivalvular involvement [2,10–13]. In fact, ^{18}F FDG PET/CT imaging maintained a sensitivity and specificity of 86% and 84%, respectively, in those patients who demonstrated limited echocardiography sensitivity [14]. The major contribution of this imaging modality occurs in those cases where there is a high suspicion of IE and with a diagnosis of "Possible IE" or even "IE rejected" based on the other diagnostic criteria [6,10,15–17]. The inclusion of the ^{18}F FDG PET/CT imaging modality in the Duke criteria increased sensitivity from 57.1% to 83.5% [8].

The standardized uptake value (SUV)-related metrics have been widely used to analyze the metabolic patterns associated with cardiovascular infectious disease [2,9,17–25]. Although experience with SUV-based semiquantitative metrics has shown extensive use in oncologic applications, their use is less widespread in infective endocarditis and there is not yet a standard to obtain consistent values across studies [9,26–28]. Despite some promising results in this regard, further technical developments are needed to consolidate the potential value of ^{18}F FDG PET/CT in the diagnosis of IE [28,29]. In addition, recent advances have shown that the uptake pattern could play a relevant role in decreasing false positives. In fact, a homogeneous uptake pattern is related to reactive inflammatory activity and not to infection. On the contrary, a heterogeneous uptake pattern with multiple foci is related to an infectious process [3,8]. The radiomic-based approaches in diagnostic imaging are increasingly expanding in the clinical setting [30–33]. This technology makes it possible to study quantitative data extracted from images and generate multivariate models that learn to identify patterns between the intensities of image voxels. Intensity changes and patterns of homogeneity or heterogeneity are related to changes in signal intensity derived from metabolic and physiological mechanisms that in turn produce changes in the tissue. These patterns, often invisible to the human eye, provide extra information for the study of uptake distribution in physiological images such as ^{18}F FDG PET. Indeed, previous

works have demonstrated a positive contribution of radiomic models in the diagnosis of IE, showing promising results [34,35].

Despite the marked increase in sensitivity resulting from the inclusion of [^{18}F]FDG PET/CT imaging in the Duke criteria [8], there is still room for improvement with regard to the false positive rate. It has been described that false positives could be related to several factors such as prolonged antibiotic treatment prior to the scan, inadequate patient preparation [36], or image artifacts due to beam scattering and hardening due to prosthetic device materials in attenuation-corrected (AC) images [3,8,29,37]. In fact, the clinical guidelines' recommendations call for special attention to diagnostic evaluation not only in AC images, but also in non-attenuation-corrected (NAC) images, especially when an implantable device or prosthetic valve is present to reduce the false positive rate [3].

The present study aims to identify potential radiomic-based biomarkers of PVE through the analysis of the valvular metabolic activity in NAC [^{18}F]FDG PET images. As such, the usefulness of NAC [^{18}F]FDG PET images is assessed, whose use is recommended by clinical guidelines for the evaluation of uptake patterns. Moreover, the use of NAC images may lead to a reduction in the false positive rate of the current criteria and previous research due to the imaging artifacts produced by prosthetic and implantable devices.

2. Materials and Methods

2.1. Image Database

The current research work involves a retrospective re-evaluation of NAC [^{18}F]FDG PET/CT scans from a previously studied cohort of patients described in [25]. The previous study report provides a comprehensive overview of the utilized methods. Briefly, a total of 20 image studies (with 9 confirmed PVE diagnoses) were collected in the Department of Nuclear Medicine of the Hospital Universitario 12 de Octubre, Madrid, between 2019 and 2021 and included in the analysis. A case-by-case tabulation of the individual subjects and their clinical outcome is detailed in Supplementary Materials Table S1.

2.2. Image Acquisition

The image acquisition protocol has been detailed previously in [25]. Nonetheless, it should be noted that only the NAC [^{18}F]FDG PET scans were eligible within this study. The recruited patients adhered to a preparation protocol to enhance FDG cardiac uptake, based on a low carbohydrate and high fat diet. Whole body images from a SIEMENS Biograph 6 True Point [^{18}F]FDG PET/CT scanner (Siemens Healthineers AG, Erlangen, Germany) with head-first supine patient orientation was utilized. The mean injected dose of [^{18}F]FDG was 308.23 ± 91.69 MBq. The reconstruction of the images led to a PET scan matrix of 168×168 pixels with 5 mm of slice thickness and 4.0728 mm for in-plane resolution and a CT scan matrix of 512×512 pixels with 0.9766 mm for pixel pitch and 12 bits per pixel.

2.3. Image Processing and Feature Extraction

All image studies were processed using our in-house tool Cardiology Software Suite (in-house version) for Image Analysis (CASSIA) [25]. A thorough description of the image processing methodology is detailed in [25]. However, a few modifications are incorporated for the processing of NAC images. Briefly, the co-registration of NAC PET and corresponding CT images is performed, followed by the adequate segmentation of the heart valve metabolic activity to analyze the metabolic patterns along the valve regions. The segmentation of the valve is performed by defining a toroidal volume of interest (VOI) that isolates the metabolically active region of the prosthetic valve ring.

Once the valvular VOI is segmented, radiomic features are extracted. The adequate computation of radiomic features may require preprocessing of the segmented VOI. According to IBSI recommendations [38], the discretization of image gray values as well as interpolation to achieve an isotropic volume must be performed prior to feature extraction. In compliance with IBSI indications, the fixed bin number (FBN) discretization algorithm

is the preferred method for arbitrary units as those in the NAC [^{18}F]FDG PET images (no re-segmentation range may be defined) [38].

In addition, some discretization and interpolation parameters such as the bin number or voxel resampling size may alter the reproducibility of the radiomic features. To this purpose, this study assessed the reproducibility of the extracted radiomic indices for the variations in these extraction parameters, in terms of the intraclass correlation coefficient (ICC), as a methodological step prior to statistical analysis for the identification of potential image-based biomarkers. The bin number (4, 8, 16, 32, and 64 bins) and voxel size ($1 \times 1 \times 1 \text{ mm}^3$, $1 \times 1 \times 2 \text{ mm}^3$, $1 \times 1 \times 3 \text{ mm}^3$, and $1 \times 1 \times 4 \text{ mm}^3$) configurations were defined in compliance with the Image Biomarker Standardization Initiative (IBSI) criteria [38] and image acquisition settings of the study population. An up-sampling approach is preferred to minimize image aliasing artifacts [38]. As stated in previous work [39], an ICC(3,1) for a two-way mixed-effects model was computed to quantify the reproducibility of the radiomic features related to variations in the bin number (Experiment 1) and voxel size (Experiment 2) parameters. A threshold of 0.82 (computed as the mean endpoint between intervals defined as good [ICC 0.75–0.9] or excellent [ICC > 0.9] feature performance [40–42]) for ICC was used to group radiomic features into sets of features showing reproducible and non-reproducible values in response to variations in the feature calculation parameter configurations.

After the reproducibility analysis, the optimal feature extraction settings of parameters are defined and radiomics data are obtained according to the selected robust extraction parameters configuration.

Finally, radiomic features were extracted from the defined volume of interest encompassing the valvular region in the original non-filtered NAC [^{18}F]FDG PET images using the open-source python package Pyradiomics [43] with the default extraction parameters, unless otherwise stated above. A total of 93 features were obtained that are categorized as follows: 18 First Order Statistics, 24 Gray Level Co-occurrence Matrix (GLCM), 16 Gray Level Run Length Matrix (GLRLM), 16 Gray Level Size Zone Matrix (GLSZM), 5 Neighboring Gray Tone Difference Matrix (NGTDM), and 14 Gray Level Dependence Matrix (GLDM).

2.4. Statistical Analysis

Quantitative variables are represented as the mean \pm standard deviation. For all analyses, only consistent features are eligible. Statistical analysis was conducted by categorizing patients based on the confirmed diagnosis of PVE.

The differences in quantitative values were evaluated by means of the Mann–Whitney U test and Benjamini Hochberg correction procedure for multiple comparison (only p values < 0.05 after Benjamini Hochberg correction were considered statistically significant). SPSS software version 19.00 (IBM Corp., Armonk, NY, USA) was employed to perform all the statistical procedures. The Synthetic Minority Over-sampling Technique (SMOTE) [44] was used to balance the dataset with respect to the diagnostic groups, increasing the effective sample size ($n = 22$) and addressing class imbalance issues. To ensure further reliability, non-parametric Spearman correlations were calculated between the remaining radiomic features post-univariate and reproducibility analyses, with highly correlated features ($\rho \geq 0.9$) discarded to mitigate multicollinearity issues (correlation coefficients are detailed in Supplementary Materials Figure S1).

Eight machine learning (ML) classification models were evaluated in Orange 3.31 software (Bioinformatics Laboratory at the University of Ljubljana, Slovenia; <https://orangedatamining.com/>, accessed on 23 February 2024) for Confirmed PVE vs. Discarded PVE classification based on the following remaining standardized radiomic features: logistic regression, neural network, k-nearest neighbor (kNN), naive bayes, support vector machine (SVM), random forest, gradient boosting, and decision tree. The model hyperparameters are summarized in Supplementary Materials Table S2. A 5-fold cross validation was performed to validate the ML models. The ML models' performance was assessed in terms of the area under the curve (AUC), accuracy, F1-score, precision, recall, and specificity. A value greater than 0.75 was considered as an indicator of acceptable model performance.

3. Results

According to the results of the reproducibility analysis (Figures 1 and 2), 95.7% (89 out of 93) of the features remain consistent when varying the voxel size (median ICC values were 0.945 [IQR 0.764–0.997] and 0.987 [IQR 0.948–0.998] for absolute agreement and consistency, respectively) whether only 45.2% (42 out of 93) of the features remain consistent for variations in the discretization bin number (median ICC values were 0.250 [IQR 0.116–0.512] and 0.793 [IQR 0.459–0.984] for absolute agreement and consistency, respectively). In compliance with IBSI recommendations and given the non-dependence relationship of the radiomic features and voxel size configuration, an isotropic volume resampling strategy with a $1.0 \times 1.0 \times 1.0 \text{ mm}^3$ voxel size was employed. Conversely, some further discrepancies could be noted within the radiomic features' values when altering the discretization bin number parameter. Therefore, the discretization bin number was set to 64 bins in compliance with IBSI standards [38].

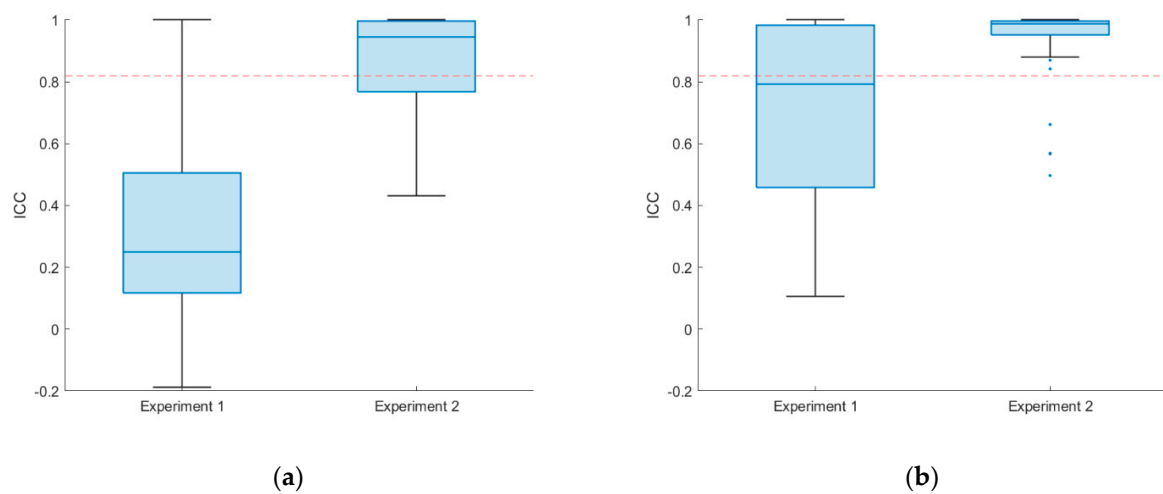


Figure 1. Absolute agreement (a) and consistency (b) ICC values of the radiomic features for the variation of the bin number (Experiment 1) and voxel size (Experiment 2) configurations.

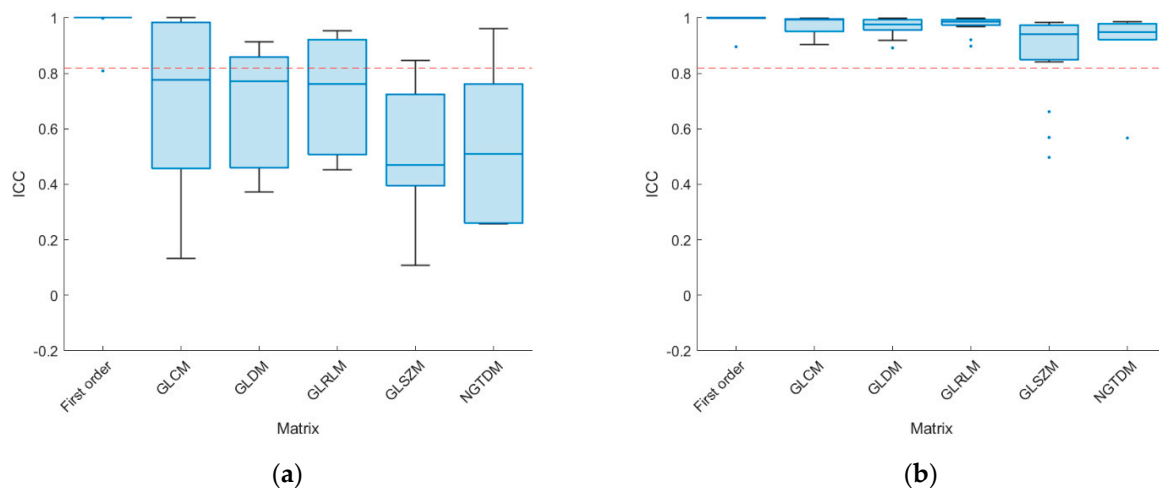


Figure 2. Consistency ICC values of the radiomic features groups for (a) the variation of the bin number (Experiment 1) and (b) the variation in voxel size (Experiment 2) configurations.

The statistically significant differences between the diagnostic PVE groups in the radiomic predictors which also maintain an ICC above the established threshold for consistency ($ICC > 0.82$) are shown in Table 1. Notably, highly correlated features ($\rho \geq 0.9$) were also discarded to mitigate multicollinearity issues (see Supplementary Materials Figure S1).

These features were acquired using the FBN method (64 bins) for gray level discretization and a voxel size of $1.0 \times 1.0 \times 1.0 \text{ mm}^3$. The statistically significant differences between PVE groups were described in a total of 2 GLRLM, 1 first order, 1 GLDM, and 1 NGTDM features. The differences between the subgroups are shown in Figure 3.

Table 1. Radiomic features with statistically significant differences between discarded and confirmed PVE.

	Feature	Discarded PVE	Confirmed PVE	p-Value	ICC [95% CI]
First order	Entropy	5.00 ± 0.07	5.39 ± 0.03	0.003 *	0.999 [0.999–1.000]
GLDM	DependenceEntropy	8.18 ± 0.02	8.49 ± 0.02	0.003 *	0.873 [0.767–0.942]
GLRLM	GrayLevelNonUniformity	648.90 ± 0.29	452.78 ± 0.38	0.025	0.910 [0.835–0.959]
	RunEntropy	5.80 ± 0.02	6.09 ± 0.03	0.003 *	0.892 [0.802–0.951]
NGTDM	Coarseness	0.0014 ± 0.001	0.002 ± 0.35	0.028	0.962 [0.930–0.983]

* Significant after Benjamini Hochberg multiple testing correction. PVE: prosthetic valve endocarditis; CI: confidence interval.

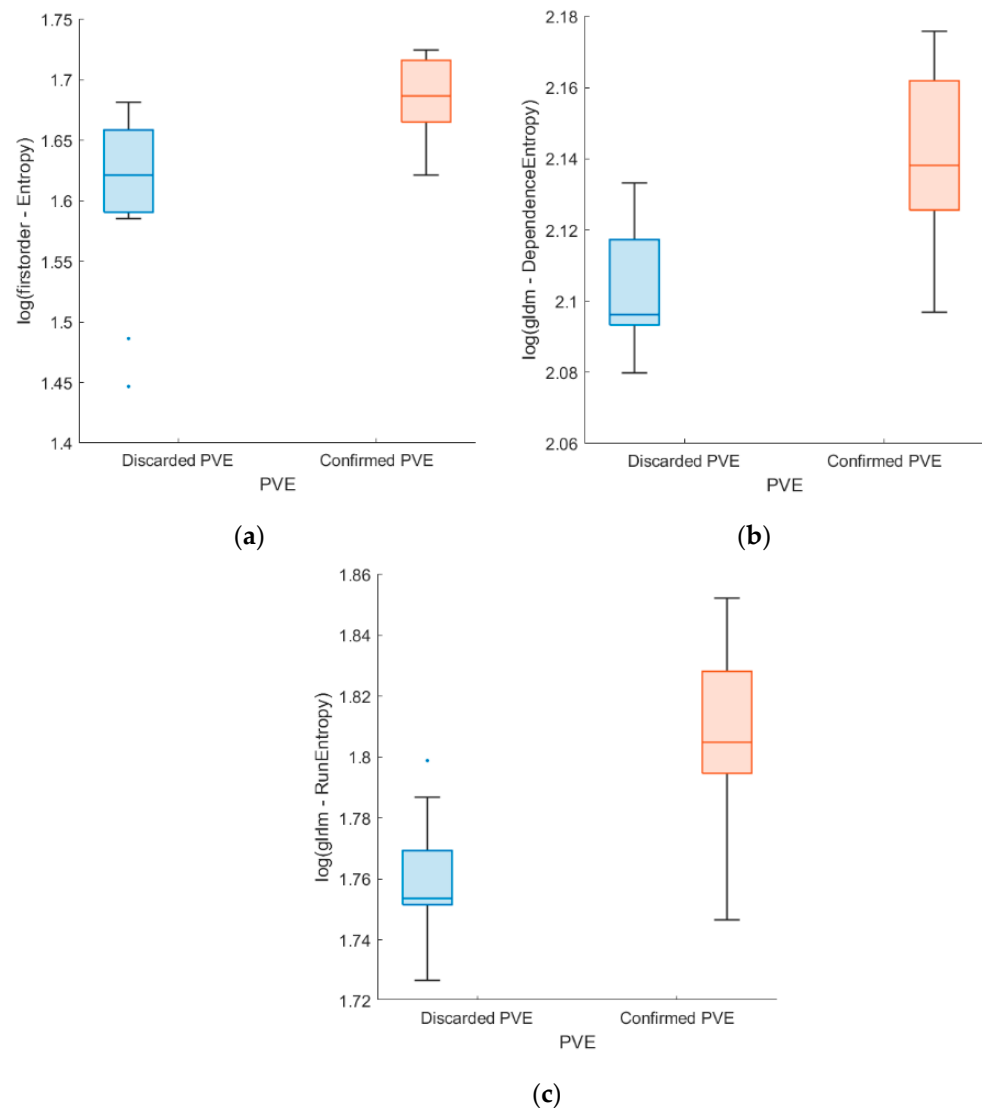


Figure 3. Boxplots of the statistically significant radiomic features after Benjamini Hochberg multiple testing correction. Log values are calculated to show the differences between the diagnostic groups (Discarded PVE vs. Confirmed PVE). (a) First order Entropy; (b) GLDM Dependence Entropy; (c) GLRLM RunEntropy.

ML models based on radiomic features with significant differences between confirmed and discarded PVE in the Mann–Whitney U test are evaluated (Table 2). Logistic regression showed an AUC of 0.876 with an overall sensitivity (recall) and specificity of 0.864 and 0.864, demonstrating a potential great capability of PVE classification. Similar performances were obtained for models based on all radiomic variables (Supplementary Materials Table S3).

Table 2. Performances of the internal validation for the ML models based on the selected radiomic features for Confirmed PVE and Discarded PVE classification.

Method	AUC	Accuracy	F1-Score	Precision	Recall	Specificity
Logistic Regression	0.876 *	0.864 *	0.863 *	0.867 *	0.864 *	0.864 *
Neural Network	0.876 *	0.818 *	0.818 *	0.818 *	0.818 *	0.818 *
SVM linear	0.860 *	0.818 *	0.818 *	0.818 *	0.818 *	0.818 *
Decision tree	0.769 *	0.682	0.681	0.683 *	0.682	0.682
Random Forest	0.839 *	0.818 *	0.817 *	0.829 *	0.818 *	0.818 *
Naive Bayes	0.855 *	0.773 *	0.768 *	0.795 *	0.773 *	0.773 *
Gradient Boosting	0.851 *	0.818 *	0.818 *	0.818 *	0.818 *	0.818 *
kNN	0.835 *	0.818 *	0.818 *	0.818 *	0.818 *	0.818 *

* Acceptable performance (>0.75).

4. Discussion

Despite recent advances and the increased sensitivity and specificity of current diagnostic criteria, IE still accounts for high morbidity and mortality [4–6,8]. [¹⁸F]FDG PET/CT imaging has recently demonstrated its high value for the screening of IE [2,6,10–17]. However, the false-positive rate remains limited in those cases where implantable devices or prosthetic valves are involved, which may produce artifacts in the non-attenuation corrected images [3,8,29,37]. In fact, clinical guidelines recommend checking imaging findings also in NAC images in order to reduce the false-positive rate [3]. Likewise, the analysis of SUV-based metrics and uptake patterns based on the homogeneity/heterogeneity of radiopharmaceutical distribution has been shown to play a relevant role in the proper diagnosis of IE [2,9,17–25]. Although these previous studies mainly propose SUV-based metrics to describe valvular uptake patterns, emerging evidence suggests that uptake heterogeneity through radiomic analysis may play a significant role in IE diagnosis. Nevertheless, despite the recent increasing applicability of radiomics in some clinical scenarios such as oncology [30–33], its usage is still scarce and poorly extended in the case of IE. Nonetheless, some studies have recently demonstrated promising results for the early detection of IE [34,35]. However, to the best of our knowledge, the present study is the first to evaluate metabolic uptake radiomic-based patterns in NAC [¹⁸F]FDG PET images in the setting of prosthetic valve infective endocarditis (PVE) to support the current diagnostic criteria, following the clinical guidelines' recommendations for the diagnosis of PVE.

In our study, a total of 22 imaging studies were evaluated, with a total of 93 imaging features per study. Additionally, a repeatability and reproducibility analysis of these radiomic features was evaluated on NAC [¹⁸F]FDG PET/CT images. Reproducibility analysis showed that some radiomic features were consistent against changes in acquisition settings. Consistency ICCs above the defined 0.82 threshold demonstrated reproducibility against variations in the bin number and interpolation thickness, respectively. Moreover, a non-dependency relationship of radiomic values with respect to variation in interpolation thickness was evidenced. Furthermore, first order, GLCM, and GLRLM features demonstrated greater consistency against variations in the number of bins. Specifically, 94.4% (17 out of 18), 43.8% (7 out of 16), and 41.7% (10 out of 24) of the first order features, GLRLM, and GLCM remained consistent over variations in the number of bins.

In the univariate analysis, five radiomic features showed statistically significant differences between the confirmed and discarded PVE (Table 1) in addition to good reproducibility of the results ($ICC > 0.82$). The differences between studies with confirmed and discarded PVE show a trend of increased entropy in studies with confirmed PVE with respect to studies with discarded PVE (Figure 3). According to the definition provided by the IBSI standard [38], entropy refers to the uncertainty/randomness of the radiomic values and, therefore, to the tissue uptake heterogeneity. That is, a higher entropy could be explained by a greater dispersion of uptake values in the studied region, whereas a reduced entropy would mean a greater uptake homogeneity. This finding is therefore in line with the results described in previous studies, where a homogeneous uptake pattern was previously related to reactive inflammatory activity and not to infection [3,8] whereas a heterogeneous uptake pattern with multiple foci is related to an infectious process. Previous studies have also demonstrated the usefulness of [^{18}F]FDG PET/CT in the assessment of patients with suspected PVIE [2,10–14]. However semi-quantitative metrics and SUV ratios are commonly assessed which may miss valuable insights into the patterns of homogeneity/heterogeneity in valvular uptake related to PVE diagnosis.

Reproducibility and univariate statistical analyses allowed to define statistically significant radiomic potential predictors for PVE classification. Subsequently, a multivariate analysis of radiomic features based on the evaluation of different ML models was performed. In accordance with the outlined criteria for translating radiomics into clinically useful tests, as detailed in previous research [45], the present study thoroughly revisited these criteria in the study design. Moreover, the CLEAR checklist for radiomics research [46] has been completed (see Supplementary files). Nonetheless, limitations were encountered, and were primarily attributed to the restricted power sample size and challenges in fulfilling the criteria associated with model development. Therefore, given the limited patient cohort and limited statistical power, only an internal validation of these models was aimed within a proof-of-concept framework, without the explicit objective of validating a clinically feasible model. Therefore, this proof-of-concept multivariate analysis aims to conduct an initial assessment of the potential value of NAC [^{18}F]FDG PET imaging in improving the accuracy of PVE diagnosis.

The ML models evaluated were constructed using the radiomic biomarkers selected in the reproducibility and univariate analyses. The logistic regression model showed the best performance within the internal validation, reaching an AUC of 0.876, with a sensitivity of 0.864 and specificity of 0.864 (Table 2). The ML models show an acceptable performance for the detection of PVE. However, all the models demonstrated comparable performance outcomes, likely due to the restricted internal validation conducted with a limited patient cohort. Further investigations with an enlarged patient cohort will be necessary to enhance model disparities and assess their potential clinical relevance and context-specific adequacy. The study by PA. Erba et al. [34] evaluated the potential of radiomic analysis on AC [^{18}F]FDG PET/CT imaging for the diagnosis of IE through predictive models for the risk stratification of patients. Clinical data, imaging data, and classification according to Duke criteria were collected in a total of 447 patients. Models that integrated further information (image-based information and clinical data) achieved higher performance (logistic regression model reached an AUC of 0.91). They established that multivariable models based on radiomics and clinical information had a positive but still limited contribution to the diagnosis of IE and stratification of patients into risk profiles. In the study by T. Godefroy et al. [35], the usefulness of ML models based on radiomic features for the diagnosis of PVE in AC [^{18}F]FDG PET/CT imaging was evaluated. Clinical and imaging data were collected from a total of 108 patients. The SVM model achieved the best performance in the classification of IE reaching an AUC of 0.79 in the model that included only radiomic features and 0.82 in the model that integrated clinical and imaging information. They established that FDG PET/CT image-based machine learning algorithms achieved acceptable performance in terms of sensitivity and specificity for IE classification.

As previously stated, the present study is a re-evaluation of the analysis performed in [25]. In the previous work, SUV-based ratios yielded patterns of heterogeneity in the valvular uptake of AC [¹⁸F]FDG PET/CT images with a performance of the valvular heterogeneity index (VHI) and ring-to-center ratio (RCR) reaching an AUC of 0.727 and 0.808, respectively. Moreover, univariate analysis demonstrated statistically significant differences between the confirmed and discarded PVE groups for the RCR index ($p = 0.02$). On the other hand, the present study demonstrates that multivariate models based on radiomic features extracted from [¹⁸F]FDG PET/CT NAC images lead to a higher performance in PVE classification (AUC = 0.876). Therefore, the preliminary findings from both univariate analysis and the multivariate models proposed in this work suggest the potential of NAC [¹⁸F]FDG PET imaging to enhance diagnostic sensitivity for IE, particularly in PVE. These results would set the basis for future validation studies that incorporate radiomic technology and ML models for the early detection of PVE. Thus, the radiomic-based biomarkers approach may provide a better diagnostic accuracy in describing valvular uptake patterns to characterize the specific pathophysiology of PVE. The inclusion of ML models in the current diagnostic criteria would potentially increase their sensitivity and specificity.

Some limitations of the present study include the retrospective and single-center nature of the investigation which may limit the generalizability of findings. Moreover, the study did not control other imaging acquisition parameters, such as the scanner type, reconstruction method, or multiple-reader segmentation reproducibility, all of which are known to impact radiomic feature values. Furthermore, the study only performed an internal validation of the multivariate models, lacking an independent test for validation. For this purpose, an estimation of the power and sample size to avoid the underdetermination or classification of the parameters [47,48] was additionally performed using G*power software version 3.1 (<https://www.psychologie.hhu.de/arbeitsgruppen/allgemeine-psychologie-und-arbeitspsychologie/gpower>, accessed on 3 March 2024) [49]. For power and sample size estimation, the parameters recommended in previous studies were employed [48]. Considering a minimum desired statistical power of 0.8, a large effect size of 0.8, an alpha value of 0.05 for the Mann–Whitney U test, and a 1:1 ratio between groups, the sample estimate obtained was a minimum of 54 patients, with 27 patients per group, to avoid the underdetermination or classification of the parameters [47]. Nevertheless, the present study utilized a limited sample of 20 imaging studies (22 observations after applying SMOTE). Thus, conducting more extensive prospective studies with a larger pool of patients is of great importance. This approach will enhance the comprehension of the clinical significance of our findings, validate their reliability, and assess the potential of ML models based on radiomic features for classifying PVE.

However, promising results concerning the radiomic-based approach have been obtained, showing an improvement in the sensitivity and specificity of SUV-based metrics in previous work, and setting the basis for future perspectives for the inclusion of ML models as part of the diagnostic criteria. Therefore, an accurate diagnosis of infective endocarditis is an important goal and there is significant potential for the radiomic-based biomarker evaluation of PVE patients.

5. Conclusions

High morbidity and mortality still occur in patients who are diagnosed with IE. Despite recent improvements in diagnostic criteria due to the incorporation of medical imaging as one of the major criteria, there is still some ambiguity in the protocols, as well as a high false positive rate in the case of PVE, leaving room for improvement. Radiomic technology based on the information extracted from the images may lead to a significant improvement in the early detection of PVE, with a consequent enhancement in the sensitivity and specificity of the current diagnostic criteria. In the present study, the utility of potential radiomic-based biomarkers in the diagnosis of PVE in NAC [¹⁸F]FDG PET/CT images has been evaluated. While initial findings indicate that a radiomic-based approach holds promise

for enhancing PVE diagnostic sensitivity, future studies will be required to validate the use of this technology as a valuable tool to support the current PVE diagnostic criteria.

Supplementary Materials: The following supporting information can be downloaded at: <https://www.mdpi.com/article/10.3390/app14062296/s1>, Table S1: Case-by-case tabulation of the individual subjects and their clinical outcome. Table S2: Hyperparameters of the ML models for Confirmed PVE and Discarded PVE classification.; Table S3: Performances of ML models based on all the extracted radiomic features for Confirmed PVE and Discarded PVE classification. Figure S1: Non-parametric Spearman correlations were calculated between the remaining radiomic features post-univariate and reproducibility analyses, with highly correlated features ($\rho \geq 0.9$) discarded to mitigate multicollinearity issues.

Author Contributions: Conceptualization: D.P.-F., A.G.-G., A.P.S., H.B., E.J.G. and P.S.-G.; Methodology: D.P.-F., A.G.-G., A.P.S. and P.S.-G.; Software: D.P.-F. and A.P.S.; Validation: D.P.-F., A.G.-G., A.P.S. and P.S.-G.; Formal analysis: D.P.-F. and A.P.S.; Investigation: D.P.-F., A.G.-G., A.P.S., H.B., E.J.G. and P.S.-G.; Resources: A.G.-G., H.B., E.J.G. and P.S.-G.; Data Curation: D.P.-F., A.G.-G. and A.P.S.; Writing—Original Draft Preparation: D.P.-F., A.G.-G., A.P.S. and P.S.-G.; Writing—Review and Editing: D.P.-F., A.G.-G., A.P.S., H.B., E.J.G. and P.S.-G.; Visualization: D.P.-F., A.P.S. and P.S.-G.; Supervision: P.S.-G. All authors have read and agreed to the published version of the manuscript.

Funding: This study was partially funded by Sociedad Española de Cardiología (SEC/FEC-INV-BAS 22/023).

Institutional Review Board Statement: The study was conducted in accordance with the Declaration of Helsinki and approved by the Institutional Review Board (or Ethics Committee) of the Hospital Universitario 12 October (internal code 23/650).

Informed Consent Statement: Informed consent was obtained from all subjects involved in the study.

Data Availability Statement: The data presented in this study are available upon request from the corresponding authors. Clinical records will be anonymized to mask individual identities. The pre-processing scripts or settings as well as the source code for modeling are available from the corresponding author upon reasonable request.

Conflicts of Interest: The authors declare no conflicts of interest.

References

1. Holland, T.L.; Baddour, L.M.; Bayer, A.S.; Hoen, B.; Miro, J.M.; Fowler, V.G., Jr. Infective endocarditis. *Nat. Rev. Dis. Primers* **2016**, *2*, 16059. [[CrossRef](#)]
2. Tanis, W.; Scholtens, A.; Habets, J.; Brink, R.B.v.D.; van Herwerden, L.A.; Chamuleau, S.A.; Budde, R.P. Positron Emission Tomography/Computed Tomography for Diagnosis of Prosthetic Valve Endocarditis. *J. Am. Coll. Cardiol.* **2014**, *63*, 186–187. [[CrossRef](#)]
3. Habib, G.; Lancellotti, P.; Antunes, M.J.; Bongiorni, M.G.; Casalta, J.-P.; Del Zotti, F.; Dulgheru, R.; El Khoury, G.; Erba, P.A.; Jung, B.; et al. 2015 ESC Guidelines for the management of infective endocarditis: The Task Force for the Management of Infective Endocarditis of the European Society of Cardiology (ESC). Endorsed by: European Association for Cardio-Thoracic Surgery (EACTS), the European Association of Nuclear Medicine (EANM). *Eur. Heart J.* **2015**, *36*, 3075–3128. [[CrossRef](#)]
4. Habib, G.; Badano, L.; Tribouilloy, C.; Vilacosta, I.; Zamorano, J.L.; Galderisi, M.; Voigt, J.-U.; Sicari, R.; Cosyns, B.; Fox, K.; et al. Recommendations for the practice of echocardiography in infective endocarditis. *Eur. J. Echocardiogr.* **2010**, *11*, 202–219. [[CrossRef](#)]
5. Habib, G.; Derumeaux, G.; Avierinos, J.-F.; Casalta, J.-P.; Jamal, F.; Volot, F.; Garcia, M.; Lefevre, J.; Biou, F.; Maximovitch-Rodaminoff, A.; et al. Value and limitations of the duke criteria for the diagnosis of infective endocarditis. *J. Am. Coll. Cardiol.* **1999**, *33*, 2023–2029. [[CrossRef](#)]
6. Raoult, D.; Casalta, J.P.; Richet, H.; Khan, M.; Bernit, E.; Rovero, C.; Branger, S.; Gouriet, F.; Imbert, G.; Bothello, E.; et al. Contribution of Systematic Serological Testing in Diagnosis of Infective Endocarditis. *J. Clin. Microbiol.* **2005**, *43*, 5238–5242. [[CrossRef](#)]
7. Baddour, L.M.; Wilson, W.R.; Bayer, A.S.; Fowler, V.G., Jr.; Tleyjeh, I.M.; Rybak, M.J.; Barsic, B.; Lockhart, P.B.; Gewitz, M.H.; Levison, M.E.; et al. Infective Endocarditis in Adults: Diagnosis, Antimicrobial Therapy, and Management of Complications. *Circulation* **2015**, *132*, 1435–1486. [[CrossRef](#)]
8. Ferro, P.; Boni, R.; Slart, R.H.; Erba, P.A. Imaging of Endocarditis and Cardiac Device-Related Infections: An Update. *Semin. Nucl. Med.* **2023**, *53*, 184–198. [[CrossRef](#)]
9. Mahmood, M.; Saleh, O.A. The Role of 18-F FDG PET/CT in Imaging of Endocarditis and Cardiac Device Infections. *Semin. Nucl. Med.* **2020**, *50*, 319–330. [[CrossRef](#)]

10. Nuvoli, S.; Fiore, V.; Babudieri, S.; Galassi, S.; Bagella, P.; Solinas, P.; Spanu, A.; Madeddu, G. The additional role of ^{18}F -FDG PET/CT in prosthetic valve endocarditis. *Eur. Rev. Med. Pharmacol. Sci.* **2018**, *22*, 1744–1751. [[CrossRef](#)]
11. Roque, A.; Pizzi, M.N.; Fernández-Hidalgo, N.; Permanyer, E.; Cuellar-Calabria, H.; Romero-Farina, G.; Ríos, R.; Almirante, B.; Castell-Conesa, J.; Escobar, M.; et al. Morpho-metabolic post-surgical patterns of non-infected prosthetic heart valves by [^{18}F]FDG PET/CTA: “normality” is a possible diagnosis. *Eur. Heart J. Cardiovasc. Imaging* **2020**, *21*, 24–33. [[CrossRef](#)]
12. Bartoletti, M.; Tumietto, F.; Fasulo, G.; Giannella, M.; Cristini, F.; Bonfiglioli, R.; Raumer, L.; Nanni, C.; Sanfilippo, S.; Di Eusanio, M.; et al. Combined computed tomography and fluorodeoxyglucose positron emission tomography in the diagnosis of prosthetic valve endocarditis: A case series. *BMC Res. Notes* **2014**, *7*, 32–36. [[CrossRef](#)]
13. Spacek, M.; Belohlavek, O.; Votrubova, J.; Sebesta, P.; Stadler, P. Diagnostics of “non-acute” vascular prosthesis infection using ^{18}F -FDG PET/CT: Our experience with 96 prostheses. *Eur. J. Nucl. Med.* **2009**, *36*, 850–858. [[CrossRef](#)]
14. Kamani, C.H.; Allenbach, G.; Ireige, M.; Pavon, A.G.; Meyer, M.; Testart, N.; Firsova, M.; Vieira, V.F.; Boughdad, S.; Lalonde, M.N.; et al. Diagnostic Performance of ^{18}F -FDG PET/CT in Native Valve Endocarditis: Systematic Review and Bivariate Meta-Analysis. *Diagnostics* **2020**, *10*, 754. [[CrossRef](#)]
15. Lamas, C.C.; Fournier, P.-E.; Zappa, M.; Brandão, T.J.D.; Januário-Da-Silva, C.A.; Correia, M.G.; Barbosa, G.I.F.; Golebiovski, W.F.; Weksler, C.; Lepidi, H.; et al. Diagnosis of blood culture-negative endocarditis and clinical comparison between blood culture-negative and blood culture-positive cases. *Infection* **2016**, *44*, 459–466. [[CrossRef](#)]
16. Prendergast, B.D. Diagnostic criteria and problems in infective endocarditis. *Heart* **2004**, *90*, 611–613. [[CrossRef](#)]
17. Mahmood, M.; Kendi, A.T.; Ajmal, S.; Farid, S.; O’horu, J.C.; Chareonthaitawee, P.; Baddour, L.M.; Sohail, M.R. Meta-analysis of ^{18}F -FDG PET/CT in the diagnosis of infective endocarditis. *J. Nucl. Cardiol.* **2019**, *26*, 922–935. [[CrossRef](#)]
18. Abikhzer, G.; Martineau, P.; Grégoire, J.; Finnerty, V.; Harel, F.; Pelletier-Galarneau, M. [^{18}F]FDG-PET CT for the evaluation of native valve endocarditis. *J. Nucl. Cardiol.* **2020**, *29*, 158–165. [[CrossRef](#)]
19. Granados, U.; Fuster, D.; Pericas, J.M.; Llopis, J.L.; Ninot, S.; Quintana, E.; Almela, M.; Paré, C.; Tolosana, J.M.; Falces, C.; et al. Diagnostic Accuracy of ^{18}F -FDG PET/CT in Infective Endocarditis and Implantable Cardiac Electronic Device Infection: A Cross-Sectional Study. *J. Nucl. Med.* **2016**, *57*, 1726–1732. [[CrossRef](#)]
20. Yeh, C.; Liou, J.; Chen, S.; Chen, Y. Infective endocarditis detected by ^{18}F -fluoro-2-deoxy-d-glucose positron emission tomography/computed tomography in a patient with occult infection. *Kaohsiung J. Med. Sci.* **2011**, *27*, 528–531. [[CrossRef](#)]
21. Aghayev, A. Utilization of FDG-PET/CT in the diagnosis of native valve endocarditis: There is a hope, but we need more data! *J. Nucl. Cardiol.* **2020**, *29*, 3455–3457. [[CrossRef](#)]
22. Fukuchi, K.; Ishida, Y.; Higashi, M.; Tsunekawa, T.; Ogino, H.; Minatoya, K.; Kiso, K.; Naito, H. Detection of aortic graft infection by fluorodeoxyglucose positron emission tomography: Comparison with computed tomographic findings. *J. Vasc. Surg.* **2005**, *42*, 919–925. [[CrossRef](#)]
23. Dilsizian, V.; Chandrashekar, Y. Distinguishing Active Vasculitis from Sterile Inflammation and Graft Infection. *JACC Cardiovasc. Imaging* **2017**, *10*, 1085–1087. [[CrossRef](#)]
24. Pizzi, M.N.; Roque, A.; Fernández-Hidalgo, N.; Cuellar-Calabria, H.; Ferreira-González, I.; González-Alujas, M.T.; Oristrell, G.; Gracia-Sánchez, L.; González, J.J.; Rodríguez-Palomares, J.; et al. Improving the Diagnosis of Infective Endocarditis in Prosthetic Valves and Intracardiac Devices with ^{18}F -Fluorodeoxyglucose Positron Emission Tomography/Computed Tomography Angiography. *Circulation* **2015**, *132*, 1113–1126. [[CrossRef](#)]
25. Palomino-Fernández, D.; Gómez-Grande, A.; Fernández-Igarza, M.; Pilkington, P.; Seiffert, A.P.; Bueno, H.; Gómez, E.J.; Sánchez-González, P. CASSIA (cardiology software suite for image analysis): A potential new tool for the evaluation of [^{18}F]FDG PET/CT in the setting of infective endocarditis. *Int. J. Comput. Assist. Radiol. Surg.* **2022**, *18*, 157–169. [[CrossRef](#)]
26. Scholtens, A.M.; Swart, L.E.; Kolste, H.J.T.; Budde, R.P.J.; Lam, M.G.E.H.; Verberne, H.J. Standardized uptake values in FDG PET/CT for prosthetic heart valve endocarditis: A call for standardization. *J. Nucl. Cardiol.* **2018**, *25*, 2084–2091. [[CrossRef](#)]
27. Roy, S.G.; Akhtar, T.; Bandyopadhyay, D.; Ghosh, R.K.; Hagau, R.; Ranjan, P.; Gerard, P.; Jain, D. The Emerging Role of FDG PET/CT in Diagnosing Endocarditis and Cardiac Device Infection. *Curr. Probl. Cardiol.* **2023**, *48*, 101510. [[CrossRef](#)]
28. Yan, J.; Zhang, C.; Niu, Y.; Yuan, R.; Zeng, X.; Ge, X.; Yang, Y.; Peng, X. The role of ^{18}F -FDG PET/CT in infectious endocarditis: A systematic review and meta-analysis. *Int. J. Clin. Pharmacol. Ther.* **2016**, *54*, 337–342. [[CrossRef](#)]
29. Hove, D.T.; Slart, R.; Sinha, B.; Glaudemans, A.; Budde, R. ^{18}F -FDG PET/CT in Infective Endocarditis: Indications and Approaches for Standardization. *Curr. Cardiol. Rep.* **2021**, *23*, 130. [[CrossRef](#)]
30. Guiot, J.; Vaidyanathan, A.; Deprez, L.; Zerka, F.; Danthine, D.; Frix, A.N.; Lambin, P.; Bottari, F.; Tsoutzidis, N.; Miraglio, B.; et al. A review in radiomics: Making personalized medicine a reality via routine imaging. *Med. Res. Rev.* **2022**, *42*, 426–440. [[CrossRef](#)]
31. Lambin, P.; Leijenaar, R.T.H.; Deist, T.M.; Peerlings, J.; De Jong, E.E.C.; Van Timmeren, J.; Sanduleanu, S.; Larue, R.T.H.M.; Even, A.J.G.; Jochems, A.; et al. Radiomics: The bridge between medical imaging and personalized medicine. *Nat. Rev. Clin. Oncol.* **2017**, *14*, 749–762. [[CrossRef](#)]
32. Rogers, W.; Seetha, S.T.; Refaee, T.A.G.; Lieverse, R.I.Y.; Granzier, R.W.Y.; Ibrahim, A.; Keek, S.A.; Sanduleanu, S.; Primakov, S.P.; Beuque, M.P.L.; et al. Radiomics: From qualitative to quantitative imaging. *Br. J. Radiol.* **2020**, *93*, 1108. [[CrossRef](#)]
33. Currie, G.; Hawk, K.E.; Rohren, E.; Vial, A.; Klein, R. Machine Learning and Deep Learning in Medical Imaging: Intelligent Imaging. *J. Med. Imaging Radiat. Sci.* **2019**, *50*, 477–487. [[CrossRef](#)]

34. Erba, P.; Sollini, M.; Zanca, R.; Cavinato, L.; Ragni, A.; Hove, D.T.; Glaudemans, A.; Pizzi, M.; Roque, A.; Ieva, F.; et al. [¹⁸F]FDG-PET/CT radiomics in patients suspected of infective endocarditis. *Eur. Heart J. Cardiovasc. Imaging* **2022**, *23*, jeab289.443. [[CrossRef](#)]
35. Godefroy, T.; Frécon, G.; Asquier-Khati, A.; Mateus, D.; Lecomte, R.; Rizkallah, M.; Piriou, N.; Jamet, B.; Le Tourneau, T.; Pallardy, A.; et al. ¹⁸F-FDG-Based Radiomics and Machine Learning. *JACC Cardiovasc. Imaging* **2023**, *16*, 951–961. [[CrossRef](#)]
36. Williams, G.; Kolodny, G.M. Suppression of Myocardial ¹⁸F-FDG Uptake by Preparing Patients with a High-Fat, Low-Carbohydrate Diet. *Am. J. Roentgenol.* **2008**, *190*, W151–W156. [[CrossRef](#)]
37. Scholtens, A.M.; Verberne, H.J. Attenuation correction and metal artifact reduction in FDG PET/CT for prosthetic heart valve and cardiac implantable device endocarditis. *J. Nucl. Cardiol.* **2018**, *25*, 2172–2173. [[CrossRef](#)]
38. Zwanenburg, A.; Vallières, M.; Abdalah, M.A.; Aerts, H.J.W.L.; Andrearczyk, V.; Apte, A.; Ashrafinia, S.; Bakas, S.; Beukinga, R.J.; Boellaard, R.; et al. The Image Biomarker Standardization Initiative: Standardized Quantitative Radiomics for High-Throughput Image-based Phenotyping. *Radiology* **2020**, *295*, 328–338. [[CrossRef](#)]
39. Palomino-Fernández, D.; Seiffert, A.P.; Gómez-Grande, A.; López-Guarch, C.J.; Moreno, G.; Bueno, H.; Gómez, E.J.; Sánchez-González, P. Robustness of [¹⁸F]FDG PET/CT radiomic analysis in the setting of drug-induced cardiotoxicity. *Comput. Methods Programs Biomed.* **2024**, *244*, 107981. [[CrossRef](#)]
40. Jensen, L.J.; Kim, D.; Elgeti, T.; Steffen, I.G.; Hamm, B.; Nagel, S.N. Stability of Radiomic Features across Different Region of Interest Sizes—A CT and MR Phantom Study. *Tomography* **2021**, *7*, 238–252. [[CrossRef](#)]
41. Van Velden, F.H.P.; Kramer, G.M.; Frings, V.; Nissen, I.A.; Mulder, E.R.; de Langen, A.J.; Hoekstra, O.S.; Smit, E.F.; Boellaard, R. Repeatability of Radiomic Features in Non-Small-Cell Lung Cancer [¹⁸F]FDG-PET/CT Studies: Impact of Reconstruction and Delineation. *Mol. Imaging Biol.* **2016**, *18*, 788–795. [[CrossRef](#)]
42. Sanchez, L.E.; Rundo, L.; Gill, A.B.; Hoare, M.; Serrao, E.M.; Sala, E. Robustness of radiomic features in CT images with different slice thickness, comparing liver tumour and muscle. *Sci. Rep.* **2021**, *11*, 8262. [[CrossRef](#)]
43. Van Griethuysen, J.J.M.; Fedorov, A.; Parmar, C.; Hosny, A.; Aucoin, N.; Narayan, V.; Beets-Tan, R.G.H.; Fillion-Robin, J.C.; Pieper, S.; Aerts, H.J.W.L. Computational radiomics system to decode the radiographic phenotype. *Cancer Res.* **2017**, *77*, e104–e107. [[CrossRef](#)]
44. Chawla, N.V.; Bowyer, K.W.; Hall, L.O.; Kegelmeyer, W.P. SMOTE: Synthetic Minority Over-sampling Technique. *J. Artif. Intell. Res.* **2002**, *30*, 321–357. [[CrossRef](#)]
45. Huang, E.P.; O’connor, J.P.B.; McShane, L.M.; Giger, M.L.; Lambin, P.; Kinahan, P.E.; Siegel, E.L.; Shankar, L.K. Criteria for the translation of radiomics into clinically useful tests. *Nat. Rev. Clin. Oncol.* **2023**, *20*, 69–82. [[CrossRef](#)]
46. Kocak, B.; Baessler, B.; Bakas, S.; Cuocolo, R.; Fedorov, A.; Maier-Hein, L.; Mercaldo, N.; Müller, H.; Orhac, F.; dos Santos, D.P.; et al. CheckList for EvaluAtion of Radiomics research (CLEAR): A step-by-step reporting guideline for authors and reviewers endorsed by ESR and EuSoMII. *Insights Imaging* **2023**, *14*, 75. [[CrossRef](#)]
47. Serdar, C.C.; Cihan, M.; Yücel, D.; Serdar, M.A. Sample size, power and effect size revisited: Simplified and practical approaches in pre-clinical, clinical and laboratory studies. *Biochem. Med.* **2021**, *31*, 27–53. [[CrossRef](#)]
48. Lin, W.-J.; Hsueh, H.-M.; Chen, J.J. Power and sample size estimation in microarray studies. *BMC Bioinform.* **2010**, *11*, 48. [[CrossRef](#)]
49. Faul, F.; Erdfelder, E.; Lang, A.-G.; Buchner, A. G*Power 3: A flexible statistical power analysis program for the social, behavioral, and biomedical sciences. *Behav. Res. Methods* **2007**, *39*, 175–191. [[CrossRef](#)]

Disclaimer/Publisher’s Note: The statements, opinions and data contained in all publications are solely those of the individual author(s) and contributor(s) and not of MDPI and/or the editor(s). MDPI and/or the editor(s) disclaim responsibility for any injury to people or property resulting from any ideas, methods, instructions or products referred to in the content.